

Unfolding for Joint Channel Estimation and Symbol Detection in MIMO Communication Systems

Swati Bhattacharya¹, K.V.S. Hari¹, Yonina C. Eldar²

¹ Statistical Signal Processing Lab, Department of Electrical Communication Engineering,
Indian Institute of Science, Bangalore, India.

² Faculty of Math and Computer Science, Weizmann Institute of Science, Israel.
Email: ¹{swatibh, hari}@iisc.ac.in, ²{yonina.eldar@weizmann.ac.il}

Abstract—This paper proposes a Joint Channel Estimation and Symbol Detection (JED) scheme for Multiple-Input Multiple-Output (MIMO) wireless communication systems. Our proposed method for JED using Alternating Direction Method of Multipliers (JED-ADMM) and its model-based neural network version JED using Unfolded ADMM (JED-U-ADMM) markedly improve the symbol detection performance over JED using Alternating Minimization (JED-AM) for a range of MIMO antenna configurations. Both proposed algorithms exploit the non-smooth constraint, that occurs as a result of the Quadrature Amplitude Modulation (QAM) data symbols, to effectively improve the performance using the ADMM iterations. The proposed unfolded network JED-U-ADMM consists of a few trainable parameters and requires a small training set. We show the efficacy of the proposed methods for both uncorrelated and correlated MIMO channels. For certain configurations, the gain in SNR for a desired BER of 10^{-2} for the proposed JED-ADMM and JED-U-ADMM is upto 4 dB and is also accompanied by a significant reduction in computational complexity of upto 75%, depending on the MIMO configuration, as compared to the complexity of JED-AM.

Index Terms—MIMO, wireless, communication, detection, channel estimation, ADMM, unfolding

I. INTRODUCTION

Massive multiple-input multiple-output (MIMO) systems with tens or hundreds of antennas at both the transmitter and receiver have emerged as a promising technique for achieving high spectral efficiency [1]. The conventional MIMO configuration has a larger number of receive antennas at the base station (BS) than the number of transmit antennas at the users (UEs). With the rise of fifth-generation wireless communication, an emerging scenario is where many users connect to a single BS with limited antennas i.e., $N \leq K$, referred to as overloaded MIMO [2]–[8].

One of the critical aspects in utilizing the full potential of massive MIMO is accurate symbol detection at the BS for which Maximum Likelihood (ML) detection is optimal but computationally prohibitive. Linear detectors such as Zero Forcing (ZF), Minimum Mean Square Error (MMSE) or more advanced nonlinear detectors [9], [10] and deep learning based detectors [11], [12] perform well when N is much larger than K but quickly deteriorate in performance as the ratio N/K approaches 1 which is the overloaded MIMO regime.

Symbol detection for overloaded MIMO has been studied in the literature using sparsity [2]–[4], convex optimization [5] and deep learning [6]–[8], [13].

Traditionally, the tasks of channel estimation and symbol detection are decoupled and performed separately using two independent modules in cascade, in which Channel State Information (CSI) is first estimated followed by symbol detection. Joint Channel Estimation and Symbol Detection (JED) methods [14]–[18] consider the transmitted data as additional pilots, and exchange information iteratively between the two aforesaid modules as depicted in Fig. 1, thereby resulting in better channel and symbol estimates. Message passing based techniques for JED were proposed in [14]–[17], however, they depend heavily on the channel sparsity and data statistics and require extensive probability calculations. In contrast, a simple iterative technique for JED presented in [18], which is based on Alternating Minimization (AM), updates the channel and symbols using MMSE-based and ZF estimates, respectively. We refer to the technique proposed in [18] as JED-AM and provide further details in Section III-B.

Deep Unfolding, a model-based neural network providing interpretability with reduced number of tunable parameters and training, was introduced in the seminal work of Gregor and LeCun in [19] and has gained attention over the last few years. These neural networks which are derived from a parent iterative algorithm are shown to improve the performance over fully-connected black-box detectors along with reduced computational complexity [6]–[8], [11]–[13], [20]–[32] and have been widely used in the domain of image processing [20]–[23].

In the context of wireless communications, unfolding has been used for symbol detection assuming knowledge of CSI, [6]–[8], [11], [12], [25]–[27] and for jointly obtaining the channel and symbol estimates [13], [24], [33], [34]. One of the first works presented a deep unfolded version of Orthogonal AMP (OAMP), named OAMP-Net2, in [13]. An unfolded soft-output based symbol detection method is outlined in [24]. A more recent work in [34] base their unfolded network on the Expectation-Maximization (EM) algorithm. A related work on JED is presented in [33] which uses a convolutional neural network instead of a model-based unfolded network.

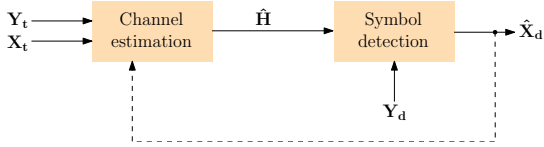


Fig. 1: A generic JED architecture with channel estimation and symbol detection blocks that iteratively exchange information until convergence.

Our main contributions are summarized as follows:

- The first algorithm, JED-ADMM, exploits the property of the data symbols being in the Quadrature Amplitude Modulation (QAM) constellation to impose a non-smooth constraint and propose an equivalent ADMM formulation for JED. We see from the simulation studies of Section VI-B1 that JED-ADMM results in an improved bit error rate (BER) performance over the existing JED-AM [18]. The performance of ADMM-based algorithms greatly depends on the penalty parameter [35]. We see that the BER yielded by JED-ADMM is also affected by the ADMM penalty parameter, which is decided empirically. To mitigate the loss in performance that could possibly be caused by an improper choice of the ADMM penalty parameter, we let it be trained from the data leading to the next algorithm.
- The second algorithm unfolds the ADMM iterations of JED-ADMM to build a model-based network (JED-U-ADMM). We also introduce some additional trainable parameters, otherwise not included in JED-ADMM, to construct a flexible unfolded network. Simulation studies in Section VI-B2 demonstrate the improvement in performance as well as reduction in computational complexity.
- We note that the previous works on JED, that use unfolding, demonstrate the performance of their algorithms for either $N > K$ in [24], $N = K$ in [13] or $N \geq K$ as in [34]. In contrast, we provide simulation studies for JED-ADMM and JED-U-ADMM in all possible MIMO configurations $N > K$ and $N \leq K$.

We describe the system model and existing JED in Sections II and III-B respectively. The reformulation via ADMM is in Section IV-A and its deep unfolded version in Section V-A. Simulation parameters for our experiments are described in Section VI-A and the experimental results for our proposed approach are detailed in Section VI-B.

Throughout the paper we use the following notation: Bold-faced uppercase and lowercase letters \mathbf{A} , \mathbf{a} and plain faced letters a represent a matrix, column vector and scalar respectively. The conjugate-transpose and the Moore-Penrose pseudoinverse of \mathbf{A} are given by \mathbf{A}^* , \mathbf{A}^\dagger respectively. The symbol \mathbb{S}_β is the constellation for β -QAM and \mathbf{I}_n is the $n \times n$ identity matrix. The normal distribution with mean μ and variance σ^2 is given by $x \sim \mathcal{CN}(\mu, \sigma^2)$ and $x \sim \mathcal{U}[a, b]$ is the continuous uniform distribution on $[a, b]$. We use $\mathcal{P}_{\infty, \sqrt{\beta}}(\mathbf{X})$ to denote the element-wise projection of \mathbf{X} onto the infinity-norm ball of radius $\sqrt{\beta}$ and $\mathbb{1}$ is the indicator function. The list of symbols and acronyms used in the paper are summarized

in Tables I and II, respectively.

II. SYSTEM MODEL AND PROBLEM FORMULATION

Consider the uplink transmission in a narrow-band MIMO system with N BS antennas and K single-antenna users, as depicted in Fig. 2. The channel is considered to have a block

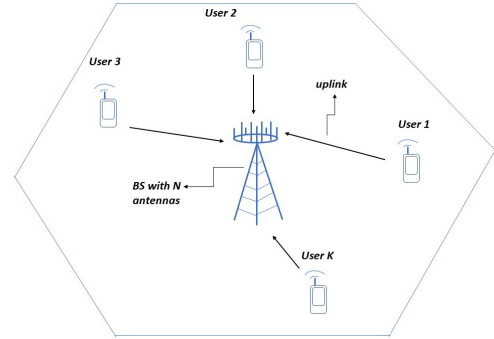


Fig. 2: Uplink MIMO communication scenario with N antennas at the BS and K single-antenna UEs.

fading structure and remains constant over T transmissions. The first T_t symbols are pilot symbols used to obtain an initial estimate of CSI and the remaining $T_d = T - T_t$ symbols are for data i.e., $\mathbf{X}_t \in \mathbb{C}^{K \times T_t}$ is the transmitted pilot matrix and $\mathbf{X}_d \in \mathbb{C}^{K \times T_d}$ is the transmitted data matrix. At the n^{th} instant, user k transmits data $\{x_k(n) \in \mathbb{S}_\beta : n \in \{1, 2, \dots, T_d\}\}$. Here, \mathbb{S}_β is the rectangular β -QAM constellation with real and imaginary parts in $\{-\sqrt{\beta} + 1, -\sqrt{\beta} + 3, \dots, \sqrt{\beta} - 3, \sqrt{\beta} - 1\}$. We consider two channel models:- (a) a Rayleigh fading channel $\mathbf{H} \in \mathbb{C}^{N \times K}$ with elements drawn from the Gaussian distribution $\mathbf{H} \sim \mathcal{CN}(\mathbf{0}, \sigma_h^2 \mathbf{I}_K)$ and (b) a correlated channel $\mathbf{H} = \mathbf{R}_r^{\frac{1}{2}} \mathbf{H}_w \mathbf{R}_t^{\frac{1}{2}}$, with \mathbf{R}_r and \mathbf{R}_t being the correlation matrices at the receiver and the transmitter respectively and \mathbf{H}_w being a Rayleigh fading channel. Let $\mathbf{V} \in \mathbb{C}^{N \times T}$ be circularly symmetric complex white Gaussian noise at the receiver; $\mathbf{V} \sim \mathcal{CN}(\mathbf{0}, \sigma_v^2 \mathbf{I}_N)$. Denoting the received pilot and data matrix by $\mathbf{Y}_t \in \mathbb{C}^{N \times T_t}$ and $\mathbf{Y}_d \in \mathbb{C}^{N \times T_d}$ respectively, the system model is as follows:

$$\mathbf{Y} = \mathbf{H}\mathbf{X} + \mathbf{V} = \mathbf{H}[\mathbf{X}_t \ \mathbf{X}_d] + [\mathbf{V}_t \ \mathbf{V}_d] = [\mathbf{Y}_t \ \mathbf{Y}_d] \quad (1)$$

where $\mathbf{X} \in \mathbb{C}^{K \times T}$ is the complete transmitted signal matrix and $\mathbf{Y} \in \mathbb{C}^{N \times T}$ is the complete received signal matrix over T transmissions.

III. BACKGROUND

A. Symbol Detection using ADMM

Symbol detection, assuming perfect CSI, using ADMM has previously been studied in [36] where the idea of introducing an auxiliary variable for solving a non-smooth convex problem was shown to enhance the performance.

Symbol	Definition	Symbol	Definition
L	Number of iterations/layers in the unfolded network	\mathbb{S}_β	rectangular β -QAM constellation
N	Number of BS antennas	K	Number of single-antenna UEs
T_t	Number of pilot symbols	T_d	Number of data symbols
\mathbf{H}	channel between all the K UEs and the BS with N antennas	\mathbf{X}_d	data matrix transmitted from K UEs over T_d time instants
\mathbf{X}_t	pilot matrix transmitted from K UEs over T_t time instants	\mathbf{V}	noise matrix at the receiver
\mathbf{Y}_t	pilot matrix received at BS over T_t time instants	\mathbf{Y}_d	data matrix received at BS over T_d time instants
\mathcal{C}	convex hull of \mathbb{S}_β	\mathbf{Z}_d	auxiliary variable for \mathbf{X}_d
ρ_c	Spatial correlation coefficient between antennas.	Λ	dual variable for ADMM updates
ρ / ρ_l	ADMM penalty parameter for MMSE-like update of $\tilde{\mathbf{X}}_d^{(l)}$	θ / θ_l	relaxation parameter in tanh(.)
α / α_l	relaxation parameter for dual variable Λ	γ / γ_l	relaxation parameter for MMSE-like update of $\tilde{\mathbf{H}}^{(l)}$

TABLE I: List of Symbols

Symbol	Definition	Symbol	Definition
JED	Joint Channel Estimation and Symbol Detection	AM	Alternating Minimization
ADMM	Alternating Direction Method of Multipliers	DL	Deep Learning based
CSI	Channel State Information	QAM	Quadrature Amplitude Modulation

TABLE II: List of Acronyms

The task of estimating symbols $\hat{\mathbf{x}}$ from $\mathbf{y} = \mathbf{H}\mathbf{x} + \mathbf{v}$, with $\mathbf{y} \in \mathbb{C}^N$, $\mathbf{H} \in \mathbb{C}^{N \times K}$ known and $\mathbf{v} \in \mathbb{C}^N$ being the noise can be posed as (2).

$$\hat{\mathbf{x}} = \arg \min_{\mathbf{x} \in \mathbb{S}_\beta^K} \frac{1}{2} \|\mathbf{y} - \mathbf{H}\mathbf{x}\|_2^2. \quad (2)$$

The data symbol x_k , the k^{th} element of \mathbf{x} , is discrete valued with the probability mass function (pmf) : $\mathbb{P}\{x_k(n) = a\} = \frac{1}{\beta}$, $a \in \mathbb{S}_\beta$. A common relaxation is to assume that the symbols are continuous variables that are uniformly distributed over \mathcal{C} which is the convex hull of \mathbb{S}_β [18] i.e., $Re\{x_k(n)\}, Im\{x_k(n)\} \sim \mathcal{U}[-\sqrt{\beta} + 1, \sqrt{\beta} - 1]$, and

$$\mathcal{C} = \left\{ \mathbf{x} \left\| \left\| \begin{bmatrix} \text{vec}(Re\{\mathbf{x}\}) \\ \text{vec}(Im\{\mathbf{x}\}) \end{bmatrix} \right\|_\infty \leq \sqrt{\beta} - 1 \right. \right\}. \quad (3)$$

We can approximate the constraint $\mathbf{x} \in \mathbb{S}_\beta^K$ being in QAM constellation by its convex polytope \mathcal{C} and hence, we can get the symbol estimates by solving (4).

$$\hat{\mathbf{x}} = \arg \min_{\mathbf{x} \in \mathcal{C}} \frac{1}{2} \|\mathbf{y} - \mathbf{H}\mathbf{x}\|_2^2. \quad (4)$$

Solving (4) using conventional interior-point method would incur huge complexity. Since the constraint set \mathcal{C} is convex and non-smooth, the authors in [36] apply the ADMM framework and rewrite the symbol detection problem as (5).

$$\hat{\mathbf{x}} = \arg \min_{\mathbf{x}, \mathbf{z} \in \mathcal{C}} \frac{1}{2} \|\mathbf{y} - \mathbf{H}\mathbf{x}\|_2^2 + g(\mathbf{z}) \quad \text{s.t.} \quad \mathbf{z} = \mathbf{x}, \quad (5)$$

where $g(\mathbf{z})$ is the indicator function on set \mathcal{C} i.e. $\mathbb{1}_{\{\mathbf{z} \in \mathcal{C}\}}$. The augmented Lagrangian, in scaled form, for (5) is

$$\mathcal{L}_\rho(\mathbf{x}, \mathbf{z}, \lambda) = \frac{1}{2} \|\mathbf{y} - \mathbf{H}\mathbf{x}\|_2^2 + \mathbb{1}_{\{\mathbf{z} \in \mathcal{C}\}} + \frac{\rho}{2} \|\mathbf{z} - \mathbf{x} - \lambda\|_2^2, \quad (6)$$

with λ being the scaled dual variable associated with the equality constraint $\mathbf{z} = \mathbf{x}$. Simulation results in [36] demonstrate that the ADMM based solution (ADMIN) outperforms

linear detectors such as MMSE-based solutions in terms of the achieved BER.

B. Joint Channel Estimation and Symbol Detection approaches

The goal of JED is to simultaneously obtain the channel and symbol estimates $\hat{\mathbf{H}}, \hat{\mathbf{X}}_d$ from the known received signal \mathbf{Y} and the short pilot sequence \mathbf{X}_t . The authors in [18] formulate the simultaneous estimation of $\hat{\mathbf{H}}$ and $\hat{\mathbf{X}}_d$ as

$$\{\hat{\mathbf{H}}, \hat{\mathbf{X}}_d\} = \arg \min_{\mathbf{H} \in \mathbb{C}^{N \times K}, \mathbf{X}_d \in \mathbb{S}_\beta^{K \times T_d}} \|\mathbf{Y}_t - \mathbf{H}\mathbf{X}_t\|_F^2 + \|\mathbf{Y}_d - \mathbf{H}\mathbf{X}_d\|_F^2 + \frac{\sigma_v^2}{\sigma_h^2} \|\mathbf{H}\|_F^2. \quad (7)$$

Solving (7) requires a combinatorial approach, due to the discrete set $\mathbb{S}_\beta^{K \times T_d}$. It is common to instead solve (8) by using the convex constraint set \mathcal{C} in (3). Accordingly, the JED optimization problem is given by:

$$\{\hat{\mathbf{H}}, \hat{\mathbf{X}}_d\} = \arg \min_{\mathbf{H}, \mathbf{X}_d} \|\mathbf{Y}_t - \mathbf{H}\mathbf{X}_t\|_F^2 + \|\mathbf{Y}_d - \mathbf{H}\mathbf{X}_d\|_F^2 + \frac{\sigma_v^2}{\sigma_h^2} \|\mathbf{H}\|_F^2 \quad \text{s.t.} \quad \mathbf{X}_d \in \mathcal{C}. \quad (8)$$

The authors of [18] use AM to solve (8) in an iterative manner with ZF for symbol estimates $\hat{\mathbf{X}}_d$ and MMSE for channel $\hat{\mathbf{H}}$, as summarized in Steps 1 and 2 of Algorithm 1.

In the next section, we propose our algorithms JED-ADMM and JED-U-ADMM.

IV. ADMM-BASED TECHNIQUES FOR JOINT CHANNEL ESTIMATION AND SYMBOL DETECTION

A. JED-ADMM

We observe from (5) that the optimization problem to obtain the symbol estimates consists of a smooth term $(\frac{1}{2} \|\mathbf{y} - \mathbf{H}\mathbf{x}\|_2^2)$ and a non-smooth term $(\mathbb{1}_{\{\mathbf{z} \in \mathcal{C}\}})$. ADMM serves as a powerful tool in such cases [35] by separating

Algorithm 1: JED-AM [18]

input : \mathbf{Y}, \mathbf{X}_t
output: $\hat{\mathbf{X}}_d, \hat{\mathbf{H}}$

Initialize $\tilde{\mathbf{H}}^{(0)} \leftarrow \mathbf{Y}_t \mathbf{X}_t^* \left(\mathbf{X}_t \mathbf{X}_t^* + \frac{\sigma_v^2}{\sigma_h^2} \mathbf{I}_K \right)^{-1}$.
for $l = 1, 2, \dots, L$ **do**
 Step 1: $\tilde{\mathbf{X}}_d^{(l)} \leftarrow \mathcal{P}_{\infty, \sqrt{\beta}} \left(\tilde{\mathbf{H}}^{(l-1)\dagger} \mathbf{Y}_d \right)$.
 Step 2: $\tilde{\mathbf{H}}^{(l)} \leftarrow$
 $\left(\mathbf{Y}_t \mathbf{X}_t^* + \mathbf{Y}_d \tilde{\mathbf{X}}_d^{(l)*} \right) \left(\mathbf{X}_t \mathbf{X}_t^* + \tilde{\mathbf{X}}_d^{(l)} \tilde{\mathbf{X}}_d^{(l)*} + \frac{\sigma_v^2}{\sigma_h^2} \mathbf{I}_K \right)^{-1}$.
end for
Final symbol and channel estimates :
 $\hat{\mathbf{X}}_d = \mathbb{S}_\beta \left(\tilde{\mathbf{X}}_d^{(L)} \right), \hat{\mathbf{H}} = \tilde{\mathbf{H}}^{(L)}$.

out the non-smooth part using an auxiliary variable. It has been observed that auxiliary variables provide better performance than existing methods without an auxiliary variable, in image processing applications [20], [37] as well as for symbol detection in wireless communication application [32], [36]. In the image processing problem, the improvement in performance was due to updating the solution vector along three variables (auxiliary variable, blurring kernel and latent sharp image), as a result of the additional auxiliary variable, instead of the original two variables. Thus, inspired by the technique in [20], [37] and the observed superior performance of ADMM over ZF/MMSE-based detectors (with perfect CSI) in [36], we propose to use ADMM for JED that updates over three variables \mathbf{H}, \mathbf{X}_d and an additional auxiliary variable, $\mathbf{Z}_d \in \mathbb{C}^{K \times T_d}$.

Reformulation of the JED optimization problem using ADMM, as presented in [38], for the original variables \mathbf{H}, \mathbf{X}_d and the auxiliary variable \mathbf{Z}_d becomes:

$$\begin{aligned} \{\hat{\mathbf{H}}, \hat{\mathbf{X}}_d, \hat{\mathbf{Z}}_d\} = \arg \min_{\mathbf{H}, \mathbf{X}_d, \mathbf{Z}_d} & \|\mathbf{Y}_t - \mathbf{H}\mathbf{X}_t\|_F^2 + \|\mathbf{Y}_d - \mathbf{H}\mathbf{X}_d\|_F^2 \\ & + \frac{\sigma_v^2}{\sigma_h^2} \|\mathbf{H}\|_F^2 + \mathbb{1}_{\{\mathbf{Z}_d \in \mathcal{C}\}} \quad s.t. \quad \mathbf{X}_d = \mathbf{Z}_d. \end{aligned} \quad (9)$$

The term $\mathbb{1}_{\{\mathbf{Z}_d \in \mathcal{C}\}}$ implies that \mathbf{Z}_d lies in the constraint set \mathcal{C} described in (3). The auxiliary variable \mathbf{Z}_d is introduced to separate the non-smooth part of the optimization problem i.e., $\mathbb{1}_{\{\mathbf{Z}_d \in \mathcal{C}\}}$.

The augmented Lagrangian for the model in (9) is

$$\begin{aligned} \tilde{\mathcal{L}}_\rho \left(\mathbf{X}_d, \mathbf{Z}_d, \boldsymbol{\Lambda}', \mathbf{H} \right) = & \|\mathbf{Y}_t - \mathbf{H}\mathbf{X}_t\|_F^2 + \|\mathbf{Y}_d - \mathbf{H}\mathbf{X}_d\|_F^2 \\ & + \frac{\rho}{2} \|\mathbf{X}_d - \mathbf{Z}_d\|_F^2 + \text{tr} \left(\boldsymbol{\Lambda}'^* (\mathbf{X}_d - \mathbf{Z}_d) \right) + \frac{\sigma_v^2}{\sigma_h^2} \|\mathbf{H}\|_F^2, \end{aligned} \quad (10)$$

where $\boldsymbol{\Lambda}'$ is the Lagrangian multiplier and $\rho > 0$ is the ADMM penalty parameter. For simplicity, we consider the scaled ADMM [35] with $\boldsymbol{\Lambda} \triangleq \frac{\boldsymbol{\Lambda}'}{\rho}$ that translates the augmented

Lagrangian in (10) to

$$\begin{aligned} \mathcal{L}_\rho \left(\mathbf{X}_d, \mathbf{Z}_d, \boldsymbol{\Lambda}, \mathbf{H} \right) = & \|\mathbf{Y}_t - \mathbf{H}\mathbf{X}_t\|_F^2 + \|\mathbf{Y}_d - \mathbf{H}\mathbf{X}_d\|_F^2 \\ & - \frac{\rho}{2} \|\boldsymbol{\Lambda}\|_F^2 + \frac{\rho}{2} \|\mathbf{X}_d - \mathbf{Z}_d + \boldsymbol{\Lambda}\|_F^2 + \frac{\sigma_v^2}{\sigma_h^2} \|\mathbf{H}\|_F^2. \end{aligned} \quad (11)$$

We next minimize $\mathcal{L}_\rho \left(\mathbf{X}_d, \mathbf{Z}_d, \boldsymbol{\Lambda}, \mathbf{H} \right)$ in (11) over the variables successively in an iterative manner as in [38]. In the l^{th} iteration, we denote $\tilde{\mathbf{X}}_d^{(l)}, \tilde{\mathbf{Z}}_d^{(l)}, \tilde{\boldsymbol{\Lambda}}_d^{(l)}, \tilde{\mathbf{H}}_d^{(l)}$, as estimates of $\mathbf{X}_d, \mathbf{Z}_d, \boldsymbol{\Lambda}_d, \mathbf{H}_d$, respectively. The first step in the l^{th} iteration is to estimate $\tilde{\mathbf{X}}_d^{(l)}$ by solving the optimization function using the estimates of other parameters from the $(l-1)^{\text{th}}$ iteration,

$$\tilde{\mathbf{X}}_d^{(l)} = \arg \min_{\mathbf{X}_d \in \mathbb{C}^{K \times T_d}} \mathcal{L}_\rho \left(\mathbf{X}_d, \tilde{\mathbf{Z}}_d^{(l-1)}, \tilde{\boldsymbol{\Lambda}}^{(l-1)}, \tilde{\mathbf{H}}^{(l-1)} \right), \quad (12)$$

whose solution, for a given ρ , is given by solving for $\nabla \mathcal{L}_\rho \left(\mathbf{X}_d, \tilde{\mathbf{Z}}_d^{(l-1)}, \tilde{\boldsymbol{\Lambda}}^{(l-1)}, \tilde{\mathbf{H}}^{(l-1)} \right) = \mathbf{0}$ that yields

$$\begin{aligned} \tilde{\mathbf{X}}_d^{(l)} = & \left(\tilde{\mathbf{H}}^{(l-1)*} \tilde{\mathbf{H}}^{(l-1)} + \frac{\rho}{2} \mathbf{I} \right)^{-1} \\ & \times \left(\tilde{\mathbf{H}}^{(l-1)*} \mathbf{Y}_d + \frac{\rho}{2} \left(\tilde{\mathbf{Z}}_d^{(l-1)} - \tilde{\boldsymbol{\Lambda}}^{(l-1)} \right) \right). \end{aligned} \quad (13)$$

Next, we estimate $\tilde{\mathbf{Z}}_d^{(l)}$ by solving the following optimization function using $\tilde{\mathbf{X}}_d^{(l)}, \tilde{\boldsymbol{\Lambda}}^{(l-1)}, \tilde{\mathbf{H}}^{(l-1)}$,

$$\tilde{\mathbf{Z}}_d^{(l)} = \arg \min_{\mathbf{Z}_d \in \mathcal{C}} \mathcal{L}_\rho \left(\tilde{\mathbf{X}}_d^{(l)}, \mathbf{Z}_d, \tilde{\boldsymbol{\Lambda}}^{(l-1)}, \tilde{\mathbf{H}}^{(l-1)} \right). \quad (14)$$

The solution is given by

$$\tilde{\mathbf{Z}}_d^{(l)} = \mathcal{P}_{\infty, \sqrt{\beta}} \left(\tilde{\mathbf{X}}_d^{(l)} + \tilde{\boldsymbol{\Lambda}}^{(l-1)} \right). \quad (15)$$

The next step is to obtain $\tilde{\boldsymbol{\Lambda}}^{(l)}$ by solving

$$\arg \min_{\boldsymbol{\Lambda} \in \mathbb{C}^{K \times T_d}} \mathcal{L}_\rho \left(\tilde{\mathbf{X}}_d^{(l)}, \tilde{\mathbf{Z}}_d^{(l)}, \boldsymbol{\Lambda}, \tilde{\mathbf{H}}^{(l-1)} \right), \quad (16)$$

whose solution is given by

$$\tilde{\boldsymbol{\Lambda}}^{(l)} = \tilde{\boldsymbol{\Lambda}}^{(l-1)} + \left(\tilde{\mathbf{X}}_d^{(l)} - \tilde{\mathbf{Z}}_d^{(l)} \right). \quad (17)$$

The final step is to obtain a solution of $\tilde{\mathbf{H}}^{(l)}$ from

$$\arg \min_{\mathbf{H} \in \mathbb{C}^{N \times K}} \mathcal{L}_\rho \left(\tilde{\mathbf{X}}_d^{(l)}, \tilde{\mathbf{Z}}_d^{(l)}, \tilde{\boldsymbol{\Lambda}}^{(l)}, \mathbf{H} \right), \quad (18)$$

which is the MMSE solution

$$\begin{aligned} \tilde{\mathbf{H}}^{(l)} = & \left(\mathbf{Y}_t \mathbf{X}_t^* + \mathbf{Y}_d \tilde{\mathbf{X}}_d^{(l)*} \right) \\ & \times \left(\mathbf{X}_t \mathbf{X}_t^* + \tilde{\mathbf{X}}_d^{(l)} \tilde{\mathbf{X}}_d^{(l)*} + \frac{\sigma_v^2}{\sigma_h^2} \mathbf{I}_K \right)^{-1}. \end{aligned} \quad (19)$$

The algorithm is summarized below with the appropriate choice of the initial value of the parameters. The final estimate is obtained after L iterations.

Algorithm 2: Algorithm for Joint Channel Estimation and Symbol Detection using ADMM (JED-ADMM)

input : \mathbf{Y}, \mathbf{X}_t
output: $\hat{\mathbf{X}}_d, \hat{\mathbf{H}}$

Initialize $\tilde{\mathbf{Z}}^{(0)} = \mathbf{0}, \tilde{\mathbf{\Lambda}}^{(0)} = \mathbf{0}, \tilde{\mathbf{H}}^{(0)} \leftarrow \mathbf{Y}_t \mathbf{X}_t^* \left(\mathbf{X}_t \mathbf{X}_t^* + \frac{\sigma_v^2}{\sigma_h^2} \mathbf{I}_K \right)^{-1}$.

for $l = 1, 2, \dots, L$ **do**

Step 1: update of \mathbf{X}_d : $\tilde{\mathbf{X}}_d^{(l)} \leftarrow \left(\tilde{\mathbf{H}}^{(l-1)*} \tilde{\mathbf{H}}^{(l-1)} + \frac{\rho}{2} \mathbf{I} \right)^{-1} \left(\tilde{\mathbf{H}}^{(l-1)*} \mathbf{Y}_d + \frac{\rho}{2} \left(\tilde{\mathbf{Z}}_d^{(l-1)} - \tilde{\mathbf{\Lambda}}^{(l-1)} \right) \right)$.

Step 2: update of \mathbf{Z}_d : $\tilde{\mathbf{Z}}_d^{(l)} \leftarrow \mathcal{P}_{\infty, \sqrt{\beta}} \left(\tilde{\mathbf{X}}_d^{(l)} + \tilde{\mathbf{\Lambda}}^{(l-1)} \right)$.

Step 3: update of $\mathbf{\Lambda}$: $\tilde{\mathbf{\Lambda}}^{(l)} \leftarrow \tilde{\mathbf{\Lambda}}^{(l-1)} + \left(\tilde{\mathbf{X}}_d^{(l)} - \tilde{\mathbf{Z}}_d^{(l)} \right)$.

Step 4: update of \mathbf{H} : $\tilde{\mathbf{H}}^{(l)} \leftarrow \left(\mathbf{Y}_t \mathbf{X}_t^* + \mathbf{Y}_d \tilde{\mathbf{X}}_d^{(l)*} \right) \left(\mathbf{X}_t \mathbf{X}_t^* + \tilde{\mathbf{X}}_d^{(l)} \tilde{\mathbf{X}}_d^{(l)*} + \frac{\sigma_v^2}{\sigma_h^2} \mathbf{I}_K \right)^{-1}$.

end for

Final symbol and channel estimates : $\hat{\mathbf{X}}_d = \mathcal{S}_\beta \left(\tilde{\mathbf{X}}_d^{(L)} \right), \hat{\mathbf{H}} = \tilde{\mathbf{H}}^{(L)}$.

B. Computational Complexity

The computational complexity in terms of Floating Point Operations (FLOPS) for the proposed JED-ADMM and existing JED-AM is presented next. We note that the multiplication of two matrices of size $m \times n$ and $n \times p$ requires mnp FLOPS and the inversion of a square matrix of size n needs n^3 FLOPS. Both JED-ADMM and JED-AM use MMSE for the channel update. However, JED-ADMM needs an extra NKT_d FLOPS per iteration for the symbol detection step. The summary of the complexity of the algorithms is given in Table III. As an example, considering $N = 16, K = 16, T_d = 512, T_t = K$, we observe that JED-ADMM requires 557056 FLOPS per iteration and JED-AM needs 425984 FLOPS, the former being ≈ 1.3 times more expensive than the latter. Considering a larger MIMO system $N = 64, K = 80, T_d = 512, T_t = K$, we find that JED-ADMM needs 14315520 FLOPS, which is ≈ 1.22 times more than that of JED-AM. Hence, we note from the above examples that as N and K increase, this difference becomes negligible because the matrix inversion steps dominate the complexity.

A concise version of our work on JED-ADMM for overloaded MIMO ($N \leq K$) systems was presented in [38]. We demonstrate, in Experiment 1 of Section VI-B1, that the proposed JED-ADMM algorithm outperforms JED-AM for properly chosen values of the ADMM penalty ρ . This variation in performance of JED-ADMM, depending on the value of ρ , motivates the development of JED-U-ADMM as detailed in Section V.

V. UNFOLDING FRAMEWORK FOR DEEP LEARNING BASED JOINT ESTIMATION AND DETECTION

We observed from Figs. 4, 5 and 6 that the choice of ρ and number of iterations are critical for JED-ADMM. To mitigate the decline in performances that could be caused by poor choice of these parameters, we propose to use deep unfolding on JED-ADMM framework by introducing trainable parameters in the update equations.

A. Unfolding of JED-ADMM

We follow the approach of [6], [13] and introduce only scalar learnable quantities to propose an unfolded network JED-U-ADMM, that is derived from the unfolding of the ADMM iterations of JED-ADMM. In Steps 1-4 of JED-ADMM (Algorithm 2) the right hand side of the equation is essentially an affine combination of two or more terms with the weighting coefficient set to 1. To allow for flexibility in the framework, we introduce additional parameters θ_l, α_l that do not necessarily restrict the weighting coefficients to 1. Furthermore, we replace the fixed quantity $\frac{\sigma_v^2}{\sigma_h^2}$ with ρ_l and γ_l which can be learnt from the data. We then learn $\rho_l, \theta_l, \alpha_l, \gamma_l$ from data.

We note that the system model as described in (1) has complex-valued variables. We recast the model using real-valued variables for ease of implementation using PyTorch [39], as:

$$\bar{\mathbf{Y}} = \bar{\mathbf{H}} \bar{\mathbf{X}} + \bar{\mathbf{V}}, \quad (20)$$

where

$$\bar{\mathbf{Y}} = \left[\text{Re}(\mathbf{Y})^T \quad \text{Im}(\mathbf{Y})^T \right]^T, \quad \bar{\mathbf{X}} = \left[\text{Re}(\mathbf{X})^T \quad \text{Im}(\mathbf{X})^T \right]^T.$$

$$\bar{\mathbf{H}} = \begin{bmatrix} \text{Re}(\mathbf{H}) & -\text{Im}(\mathbf{H}) \\ \text{Im}(\mathbf{H}) & \text{Re}(\mathbf{H}) \end{bmatrix}.$$

Similar to the pilot and data portions of \mathbf{X} in (1), we denote the respective real counterparts of pilot and data using the overline $\bar{(\cdot)}$, as $\bar{\mathbf{X}}_t, \bar{\mathbf{X}}_d, \bar{\mathbf{Y}}_t, \bar{\mathbf{Y}}_d$. The corresponding real auxiliary variable is now denoted by $\bar{\mathbf{Z}}_d$ and $\bar{\mathbf{\Lambda}}$ denotes the real dual variable for the ADMM updates.

Solving for the Lagrangian in a similar manner as in (11) with the real-valued variables of (20), we obtain

$$\begin{aligned} \mathcal{L}_\rho(\bar{\mathbf{X}}_d, \bar{\mathbf{Z}}_d, \bar{\mathbf{\Lambda}}, \bar{\mathbf{H}}) &= \|\bar{\mathbf{Y}}_t - \bar{\mathbf{H}} \bar{\mathbf{X}}_t\|_F^2 + \|\bar{\mathbf{Y}}_d - \bar{\mathbf{H}} \bar{\mathbf{X}}_d\|_F^2 \\ &\quad - \frac{\rho}{2} \|\bar{\mathbf{\Lambda}}\|_F^2 + \frac{\rho}{2} \|\bar{\mathbf{X}}_d - \bar{\mathbf{Z}}_d + \bar{\mathbf{\Lambda}}\|_F^2 + \frac{\sigma_v^2}{\sigma_h^2} \|\bar{\mathbf{H}}\|_F^2. \end{aligned} \quad (21)$$

We next minimize $\mathcal{L}_\rho(\bar{\mathbf{X}}_d, \bar{\mathbf{Z}}_d, \bar{\mathbf{\Lambda}}, \bar{\mathbf{H}})$ in (21) over the variables successively using a multi-layered neural network.

Computational complexity in terms of FLOPS for each step			
proposed JED-ADMM in Algorithm 2		JED-AM in Algorithm 1 [18]	
initial estimate $\tilde{\mathbf{H}}^{(0)}$	$NKT_t + K^2T_t + K^2N + K^3$	initial estimate $\tilde{\mathbf{H}}^{(0)}$	$NKT_t + K^2T_t + K^2N + K^3$
Steps in l^{th} iteration	FLOPS	Steps in l^{th} iteration	FLOPS
Step 1 : $\tilde{\mathbf{X}}_d^{(l)}$	$K^2N + K^3 + KNT_d + K^2T_d$	Step 1 : $\tilde{\mathbf{X}}_d^{(l)}$	$K^3 + K^2N + KNT_d + 2KT_d$
Step 2 : $\tilde{\mathbf{Z}}_d^{(l)}$	$2KT_d$	Step 2 : $\tilde{\mathbf{H}}_d^{(l)}$	$NK(T_t + T_d) + K^2(T_t + T_d) + K^2N$
Step 3 : $\tilde{\mathbf{A}}_d^{(l)}$	-		-
Step 4 : $\tilde{\mathbf{H}}_d^{(l)}$	$NK(T_t + T_d) + K^2(T_t + T_d) + K^2N$		-
Total no. of FLOPS over L iterations			
JED-ADMM	$(3K^2N + K^2(2T_d + 2T_t) + NK(2T_d + 2T_t) + 2K^3)L$	JED-AM	$(3K^2N + K^2(2T_d + 2T_t) + NK(T_d + 2T_t) + 2K^3)L$

TABLE III: Comparison of FLOPS (multiplication) required for the baseline algorithms with L denoting the number of iterations in JED-AM and JED-ADMM.

In the l^{th} layer, we denote $\tilde{\mathbf{X}}_d^{(l)}$, $\tilde{\mathbf{Z}}_d^{(l)}$, $\tilde{\mathbf{A}}_d^{(l)}$, $\tilde{\mathbf{H}}_d^{(l)}$, as estimates obtained after that layer.

Successive minimization over the variables for $\mathcal{L}_\rho(\tilde{\mathbf{X}}_d, \tilde{\mathbf{Z}}_d, \tilde{\mathbf{A}}, \tilde{\mathbf{H}})$ yield similar update equations as Steps 1-4 in Algorithm 2 with $\tilde{\mathbf{X}}_d^{(l)}$, $\tilde{\mathbf{Z}}_d^{(l)}$, $\tilde{\mathbf{A}}_d^{(l)}$, $\tilde{\mathbf{H}}_d^{(l)}$ being replaced by their real counterparts $\tilde{\mathbf{X}}_d$, $\tilde{\mathbf{Z}}_d$, $\tilde{\mathbf{A}}$, $\tilde{\mathbf{H}}$, respectively.

Network architecture: The network architecture of JED-U-ADMM network is obtained by unfolding each of the iterations of JED-ADMM. There are L cascaded layers in the network, with the same architecture, but with different trainable parameters Θ_l in each of the l^{th} layer. We provide a pictorial description of the JED-U-ADMM in Fig. 3.

For the purpose of unfolding, we introduce trainable parameters in each of the update equations in the following manner:

- In Step 1 for the MMSE-like update of $\tilde{\mathbf{X}}_d$, we replace the fixed ADMM penalty parameter ρ with ρ_l that can vary with the layers l .
- To incorporate the non-linearity of neural networks, we use the tanh activation function for the update of the auxiliary variable $\tilde{\mathbf{Z}}_d$ in Step 2, instead of $\mathcal{P}_{\infty, \sqrt{\beta}}$.
- In Step 3, the error term $\left(\tilde{\mathbf{X}}_d^{(l)} - \tilde{\mathbf{Z}}_d^{(l)}\right)$ has a coefficient of 1. We can modify it to having α_l as the coefficient and let the data decide the optimal value of α_l .
- For the MMSE-like update of $\tilde{\mathbf{H}}$ in Step 4, we replace the fixed regularization parameter $\frac{\sigma_v^2}{\sigma_h^2}$, that is dependent on the noise variance and might not always be known, with a trainable parameter γ_l .

We summarize the above steps for JED-U-ADMM in Algorithm 3. Note that for $\rho_l, \gamma_l = \frac{\sigma_v^2}{\sigma_h^2}, \alpha_l = 1$ and by replacing the tanh function with $\mathcal{P}_{\infty, \sqrt{\beta}}$ (the standard projection function in literature), we get back the JED-ADMM algorithm in Algorithm 2.

Training : The loss function for backpropagation is defined as $\mathbf{L}_\Theta = \left\| \tilde{\mathbf{X}}_d - \tilde{\mathbf{X}}_d^{(L)} \right\|_F^2$.

In the training phase of JED-U-ADMM, we start with an initial value of Θ_l which is updated in accordance with the loss function \mathbf{L}_Θ in each training epoch. The update rule for Θ_l is determined by the Adam optimizer [40]. Once the

network is trained for enough number of epochs, the weights (i.e., Θ_l values) are frozen and we use this trained network to detect/estimate the unknown data. Hence, basically the equations governing JED-U-ADMM are obtained following the framework of JED-ADMM where the parameters Θ_l are obtained in a data-driven manner.

Computational complexity : In the training phase, since JED-U-ADMM is a neural network, there is an accompanying training cost which depends on the number of trainable parameters. For the JED-U-ADMM architecture summarized in Algorithm 3, it can be seen that we have distinct trainable parameters for each of the L layers leading to the training of $4L$ parameters.

Shared parameter architecture : A variation could be to allow some of the parameters to be shared across the layers. The reasoning for this alternate unfolded architecture arises from the intuition that it is possible that the values of some of the parameters do not vary significantly across the layers. In such cases, parameter sharing can lead to reduction of training complexity while maintaining similar performance. Hence, we propose the following shared architecture, henceforth referred to as ‘JED-U-ADMM : shared Params’. The parameters $\alpha_l, \theta_l, \gamma_l$ are shared across all the L layers which effectively replaces these $3L$ parameters with just 3 trainable parameters i.e. α, θ, γ . Thus, in the Steps 2, 3, 4 of Algorithm 3, $\theta_l = \theta$, $\alpha_l = \alpha$ and $\gamma_l = \gamma$ respectively. This reduces the total trainable parameters to only $L + 4$ trainable parameters. Note that for the initial $\tilde{\mathbf{H}}^{(0)}$ update, we use γ_0 . In the estimation phase, the computational complexity of JED-ADMM and JED-U-ADMM is the same (Table III).

In the next section we study the performance of the proposed methods for different scenarios.

VI. SIMULATION RESULTS

We study the BER performance of our proposed algorithms JED-U-ADMM, JED-ADMM and JED-AM.

A. Simulation scenario:

In this paper, we consider an uplink scenario where the BS with N antennas receives signals from K UEs each with a single transmit antenna. We assume the UEs are geographically well separated and the signals propagate through independent channels.

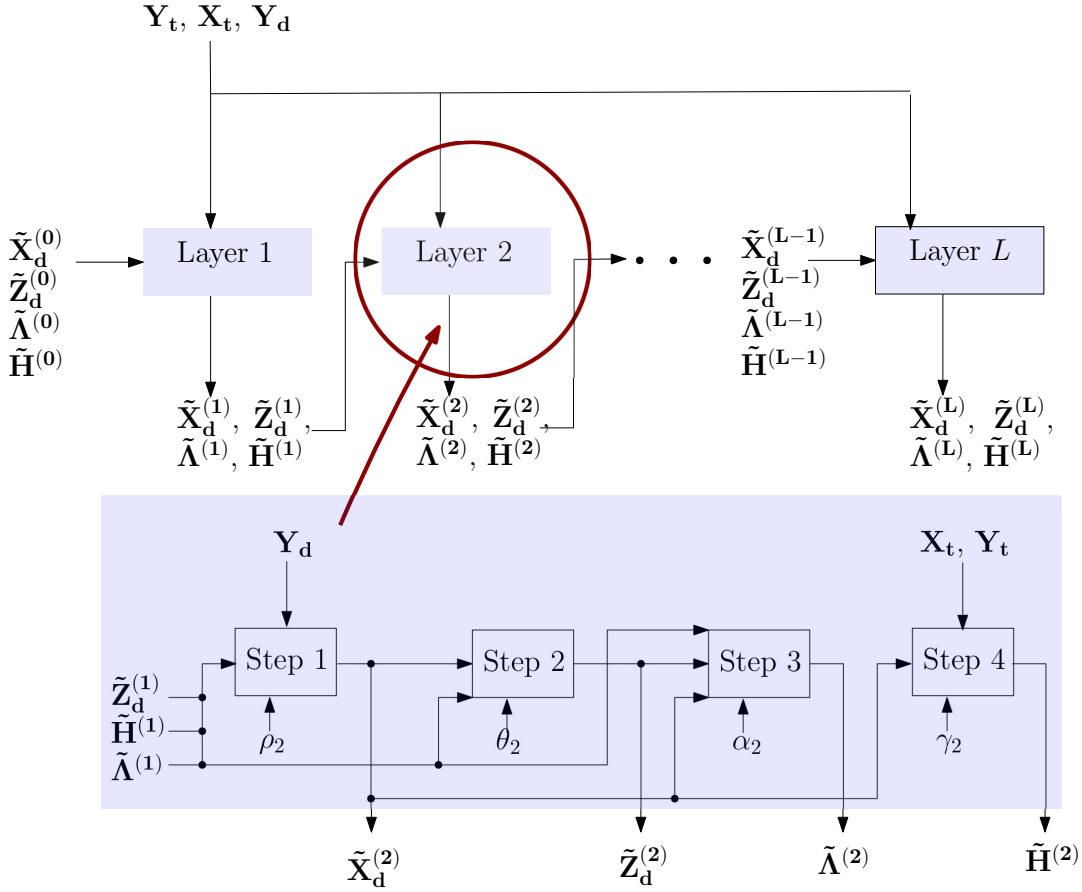


Fig. 3: Block diagram of the JED-U-ADMM architecture. There are L cascaded layers, each with 4 trainable parameters $\rho_l, \theta_l, \alpha_l, \gamma_l$. Steps 1, 2, 3, 4 refer to the corresponding steps in Algorithm 3.

Transmitter parameters: The pilot matrix \mathbf{X}_t consists of columns from the Discrete Fourier Transform (DFT) matrix and the data matrix \mathbf{X}_d is sampled from a 4-QAM ($\beta = 4$) constellation. Thus, the constellation set is given by $\mathcal{S}_\beta = \{1+j, 1-j, -1+j, -1-j\}$ and the average energy per symbol, denoted by E_s equals 2. The pilot length T_t for obtaining an initial CSI was set to the optimal pilot length required i.e., $T_t = K$.

Channel: The channel is assumed to be constant over $T = 300$ transmissions. We consider two cases of the channel: i.i.d fading Rayleigh channel, $\mathbf{H} \sim \mathcal{CN}(\mathbf{0}, \frac{1}{K}\mathbf{I})$ and correlated channels $\mathbf{H} = \mathbf{R}_r^{\frac{1}{2}} \mathbf{H}_w \mathbf{R}_t^{\frac{1}{2}}$, with \mathbf{H}_w being an i.i.d Rayleigh fading channel. The correlation matrices are \mathbf{R}_r in (22) and $\mathbf{R}_t = \mathbf{I}_K$ at the receiver and transmitter respectively [41].

$$\mathbf{R}_r = \begin{bmatrix} 1 & \rho_c & \dots & \rho_c^{K-2} & \rho_c^{K-1} \\ \rho_c & 1 & \rho_c & \dots & \rho_c^{K-2} \\ \dots & \dots & \dots & \dots & \dots \\ \rho_c^{K-1} & \rho_c^{K-2} & \dots & \dots & 1 \end{bmatrix}. \quad (22)$$

In this paper, we consider an uplink channel model which justifies the introduction of a correlation matrix at the BS antennas at the receiver. The users are assumed to be geographically separated and hence uncorrelated.

Receiver algorithms: For JED-ADMM, the receiver implements the iterative algorithms described in Algorithm 2 where L refers to the number of iterations. ρ is chosen empirically in a manner as in [36]. For the unfolded JED-U-ADMM, we use Algorithm 3 to train the network over 100/200 epochs to get the trained values of Θ_l . In the initial T_t transmissions when the transmitter sends pilots to the receiver to obtain an initial CSI, we choose a pilot structure such that only one antenna sends a pilot at a particular time instant and the rest of the antennas are turned off. During the detection phase we assume data transmitted over all antennas and use the trained Θ_l to detect symbols. For each channel realization, $T = (512 + T_t)$ bits are sent and 2×10^4 channel realizations are used. We use the PyTorch [39] environment with Adam optimizer.

Performance Metric: The performance metric to compare the algorithms is chosen to be the bit error rate (BER). We compute the BER based on errors observed in 5×10^6 bits from each of the transmitter antennas. In all the experiments, we define the Signal-to-Noise Ratio (SNR) per receiver antenna as

$$\text{SNR} = \frac{\mathbf{E} \left[\|\mathbf{H}\mathbf{X}_d\|^2 \right]}{\mathbf{E} \left[\|\mathbf{V}_d\|^2 \right]} = \frac{E_s}{\sigma_v^2}. \quad (23)$$

Algorithm 3: Proposed Algorithm for Unfolding based Joint Channel Estimation and Symbol Detection using ADMM (JED-U-ADMM)

input : $\bar{\mathbf{Y}}, \bar{\mathbf{X}}_t$
output: $\hat{\bar{\mathbf{X}}}_d, \hat{\bar{\mathbf{H}}}$

Trainable parameters : $\Theta_l = \{\rho_l, \theta_l, \alpha_l, \gamma_l\}$, $l = 1, 2, \dots, L$.

Initialize $\tilde{\bar{\mathbf{Z}}}_d^{(0)} = \mathbf{0}, \tilde{\bar{\Lambda}}^{(0)} = \mathbf{0}, \tilde{\bar{\mathbf{H}}}^{(0)} \leftarrow \bar{\mathbf{Y}}_t \bar{\mathbf{X}}_t^* (\bar{\mathbf{X}}_t \bar{\mathbf{X}}_t^* + \gamma_0 \mathbf{I}_K)^{-1}$.

for $l = 1, 2, \dots, L$ **do**

Step 1: update of $\bar{\mathbf{X}}_d$: $\tilde{\bar{\mathbf{X}}}_d^{(l)} \leftarrow \left(\tilde{\bar{\mathbf{H}}}^{(l-1)*} \tilde{\bar{\mathbf{H}}}^{(l-1)} + \rho_l \mathbf{I} \right)^{-1} \left(\tilde{\bar{\mathbf{H}}}^{(l-1)*} \bar{\mathbf{Y}}_d + \rho_l \left(\tilde{\bar{\mathbf{Z}}}_d^{(l-1)} - \tilde{\bar{\Lambda}}^{(l-1)} \right) \right)$.

Step 2: update of $\bar{\mathbf{Z}}_d$: $\tilde{\bar{\mathbf{Z}}}_d^{(l)} \leftarrow \tanh \left(\frac{\tilde{\bar{\mathbf{X}}}_d^{(l)} + \tilde{\bar{\Lambda}}^{(l-1)}}{|\theta_l|} \right)$.

Step 3: update of $\bar{\Lambda}$: $\tilde{\bar{\Lambda}}^{(l)} \leftarrow \tilde{\bar{\Lambda}}^{(l-1)} + \alpha_l \left(\tilde{\bar{\mathbf{X}}}_d^{(l)} - \tilde{\bar{\mathbf{Z}}}_d^{(l)} \right)$.

Step 4: update of $\bar{\mathbf{H}}$: $\tilde{\bar{\mathbf{H}}}^{(l)} \leftarrow \left(\bar{\mathbf{Y}}_t \bar{\mathbf{X}}_t^* + \bar{\mathbf{Y}}_d \bar{\mathbf{X}}_d^{(l)*} \right) \left(\bar{\mathbf{X}}_t \bar{\mathbf{X}}_t^* + \tilde{\bar{\mathbf{X}}}_d^{(l)} \bar{\mathbf{X}}_d^{(l)*} + \gamma_l \mathbf{I}_K \right)^{-1}$.

end for

Final symbol and channel estimates : $\hat{\bar{\mathbf{X}}}_d = \mathcal{S}_\beta \left(\tilde{\bar{\mathbf{X}}}_d^{(L)} \right), \hat{\bar{\mathbf{H}}} = \tilde{\bar{\mathbf{H}}}^{(L)}$.

B. Experiments

We consider experiments to study the performance of the proposed JED-U-ADMM, JED-ADMM and JED-AM [18] methods.

1) *Study the performance of JED-AM and JED-ADMM:*

We first study the performance of JED-ADMM and JED-AM under various MIMO configurations and channel conditions.

Experiment 1: Study the effect of varying ρ

In this experiment, we study how the choice of the ADMM penalty parameter ρ affects the BER performance of JED-ADMM. Three different MIMO configurations are considered - $N > K$, $N = K$ and $N < K$. For $N \leq K$, 20 iterations of JED-ADMM is considered while 100 iterations were taken for $N > K$. We consider two values of $\rho = \frac{\sigma_v^2}{\sigma_h^2}$ and $\rho = 4 \times \frac{\sigma_v^2}{\sigma_h^2}$.

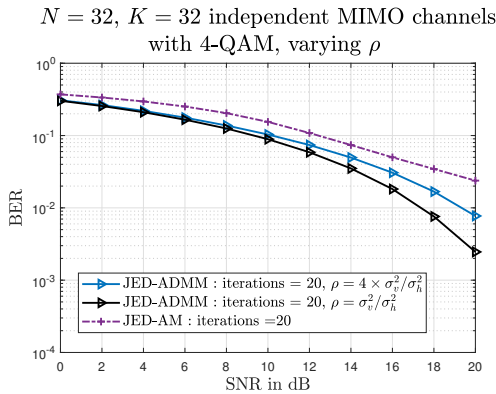


Fig. 4: $N = K$: This plot shows the variation of BER vs SNR as ρ is varied for 20 iterations of JED-ADMM and JED-AM in a 32×32 MIMO for independent Rayleigh channels.

Fig. 4 demonstrates that the choice of ρ affects the BER performance, and a lower value of ρ leads to an improvement in BER. For example, at SNR = 20 dB, with $\rho = 4 \times \frac{\sigma_v^2}{\sigma_h^2}$, we

$N = 32, K = 16$ independent MIMO channels with 4-QAM, varying ρ

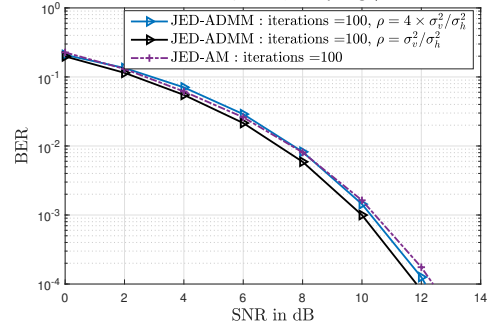


Fig. 5: $N > K$: This plot shows the variation of BER vs SNR as ρ is varied for 100 iterations of JED-ADMM and JED-AM in a 32×16 MIMO for independent Rayleigh channels.

get BER $\approx 10^{-2}$ while for $\rho = \frac{\sigma_v^2}{\sigma_h^2}$, the BER value drops to $\approx 2 \times 10^{-3}$. However, we still achieve an improvement over JED-AM irrespective of the chosen value of ρ . For $N > K$ in Fig. 5, we observe that for $\rho = 4 \times \frac{\sigma_v^2}{\sigma_h^2}$, the performance of JED-ADMM and JED-AM are very close while for $\rho = \frac{\sigma_v^2}{\sigma_h^2}$, JED-ADMM gives ≈ 0.5 dB improvement in terms of SNR at high SNR > 10 dB. We also see from Fig. 6 that for $N < K$, JED-ADMM with $\rho = \frac{\sigma_v^2}{\sigma_h^2}$ gives an order of magnitude lesser BER at SNR = 24 dB than JED-AM. On the other hand, JED-ADMM with $\rho = 4 \times \frac{\sigma_v^2}{\sigma_h^2}$ performs similarly as JED-AM.

Thus, we observe that the choice of ρ affects the BER performance of JED-ADMM which motivates us to consider letting the data decide the optimal value of ρ in a trainable setting. This is the motivation for the unfolding of JED-ADMM iterations to give us the model-based deep learning

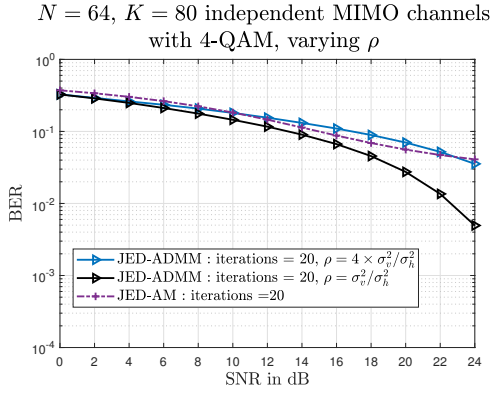


Fig. 6: $N < K$: This plot shows the variation of BER vs SNR as ρ is varied for 20 iterations of JED-ADMM and JED-AM in a 64×80 MIMO for independent Rayleigh channels.

JED-U-ADMM network.

Experiment 2: Study the effect of varying number of iterations, for a given ρ , in the presence of independent MIMO channels with $N = K$. We study the BER performance of the proposed JED-ADMM algorithm as a function of the number of iterations for the case of independent and identically distributed (i.i.d) Rayleigh channels when the number of receive antennas equals the number of transmit antennas, $N = K$ for $N = 16, 32$. The value of the ADMM penalty parameter $\rho = 4 \times \frac{\sigma_v^2}{\sigma_h^2}$ is kept constant throughout all the iterations.

In Fig. 7, we observe that with the increase in number of iterations, JED-ADMM yields a decreasing BER across all values of SNR. For example, in Fig. 7 (a), at SNR = 20 dB, 50 iterations of JED-AM gives us a BER of $\approx 10^{-2}$, whereas 50 iterations of JED-ADMM produces BER of $\approx 10^{-3}$, which is an order of magnitude lower. We also note from Figs. 7 (a) and 7 (b) that for a given number of iterations and SNR, the performance is better for lower values of $N = K$.

It is to be noted, from Fig. 7, that even as low as 10 iterations of JED-ADMM surpass 50 iterations of JED-AM. Hence, even though the number of FLOPS per iteration is slightly higher for JED-ADMM than JED-AM (Table III), we see an overall reduction in complexity owing to the lesser number of iterations needed. Accordingly, for a 16×16 MIMO as depicted in Fig. 7 (a), 50 iterations of JED-AM requires 21299200 FLOPS whereas 10 iterations of JED-ADMM requires only 5570560. Thus JED-ADMM reduces the overall FLOPS count by $\approx 75\%$ and yet achieves a lower BER.

Experiment 3: Study the effect of correlation coefficient ρ_c at the receiver with $N = K$

We investigate how JED-ADMM performs for correlated channels, that follow the Kronecker correlation channel model [41] with the correlation coefficient $\rho_c = 0.5$ and 0.9 as per (22), for the $N = K$ MIMO configuration.

We see from Fig. 8, as the correlation is decreased from $\rho_c = 0.9$ to $\rho_c = 0.5$, we see almost an order of magnitude lower BER for both JED-ADMM and JED-AM and that JED-

ADMM performs better than JED-AM for both cases. For all values of ρ_c considered and both the MIMO configurations of Figs. 8 (a) and (b), JED-ADMM consistently shows better BER performance than JED-AM. Also, for a given SNR = 20 dB and $N = K = 16$, JED-ADMM achieves BER $\approx 10^{-3}$ whereas JED-AM achieves BER $\approx 10^{-2}$ i.e., an order of magnitude improvement in BER by JED-ADMM. It is to be noted from Figs. 8 (a) and (b), that as the correlation coefficient ρ_c decreases, the gap between the performance of JED-ADMM and JED-AM also increases. For $\rho_c = 0.5$ and at an SNR = 20 dB, JED-ADMM provides a considerably lesser BER, an order of magnitude lower, than JED-AM.

2) *Study the performance of JED-ADMM and proposed deep unfolded JED-U-ADMM:* In the following experiments, we study our deep unfolded version JED-U-ADMM, in Algorithm 3, and JED-ADMM algorithm.

Experiment 4: Study the effect of sharing parameters in the presence of independent MIMO channels with $N = K$. We now study how using shared parameters (α, θ, γ) across all the L layers affects the BER performance of the unfolded network i.e. the ‘JED-U-ADMM : shared Params’ architecture. We consider 10 layers in a 16×16 MIMO system with i.i.d Rayleigh fading channel. Such a technique leads to having only $10 + 4 = 14$ trainable parameters instead of 40 trainable parameters (if there was no sharing i.e. the ‘JED-U-ADMM : unshared Params’ architecture). It can be observed in Fig. 9 that the loss in BER performance caused by the lesser number of trainable parameters in the ‘JED-U-ADMM : shared Params’ architecture is negligible, even at higher SNR > 16 dB. The reduction in number of trainable parameters is also accompanied by a reduction in the computational complexity of the unfolded network during the training phase. Hence, to simplify the architecture, in the subsequent experiments, we use only the ‘JED-U-ADMM : shared Params’ architecture.

Experiment 5: Study the effect of the number of layers on the unfolded network in the presence of independent MIMO channels with $N = K$.

In this experiment, we investigate how the BER performance of ‘JED-U-ADMM : shared Params’ changes as the number of layers is varied from 5 to 20. We consider i.i.d Rayleigh fading channel in a 16×16 MIMO system. In Fig 10, we observe that as the number of layers in increased from 5 to 15 the BER performance steadily improves. However, the network with 20 layers provides marginal improvement and therefore, in the future set of experiments with ‘JED-U-ADMM : shared Params’, we only consider the cases for 5 and 10 layers.

Experiment 6: Study the effect of unfolding in the presence of independent MIMO channels with $N = K$.

We study the BER performance of the unfolded algorithm JED-U-ADMM as a function of the number of layers of the neural network when the number of transmit and receive antennas are same in the presence of i.i.d Rayleigh fading channels. Fig. 11 demonstrates that unfolding leads to significant improvement in BER. For 16×16 MIMO in Fig. 11 (a), we observe that JED-U-ADMM with 10 layers yields an SNR improvement of 2.9 dB in achieving a BER of 10^{-2} , whereas

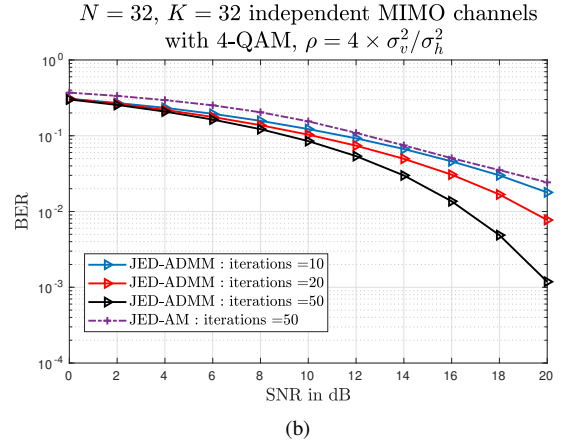
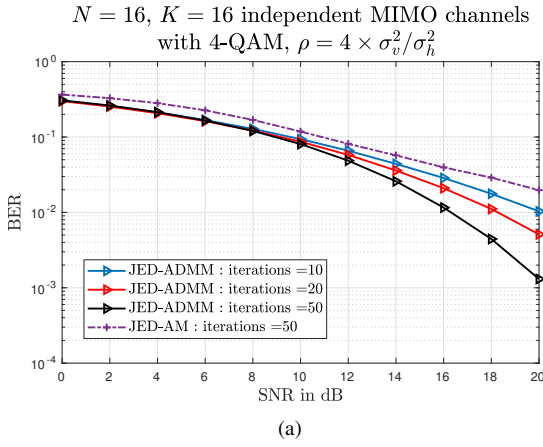


Fig. 7: This plot shows the variation of BER vs SNR depending on the number of iterations of JED-ADMM and JED-AM for (a) 16×16 and (b) 32×32 MIMO for independent Rayleigh channels.

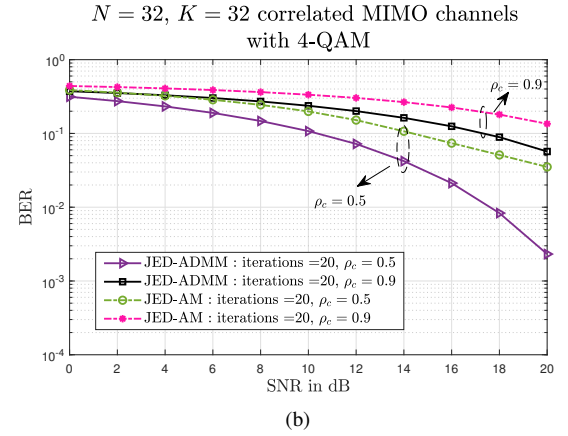
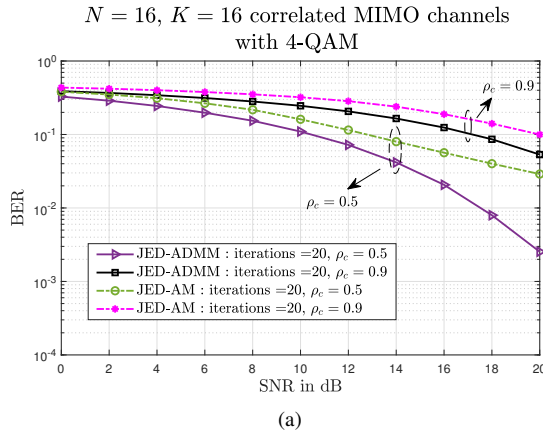


Fig. 8: This plot shows the effect of the receiver correlation coefficient ρ_c on the variation of BER vs SNR for (a) 16×16 and (b) 32×32 MIMO for JED-ADMM and JED-AM for correlated channels [41].

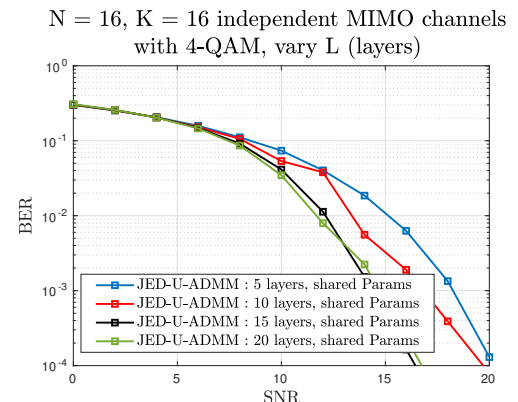
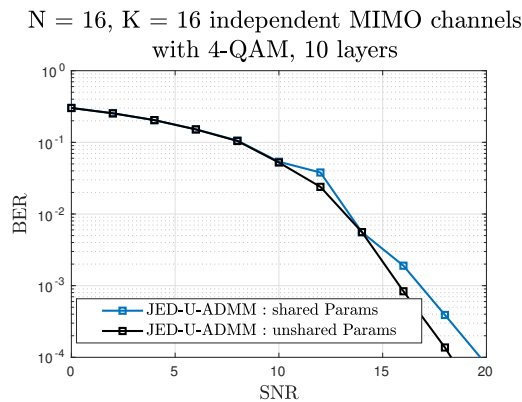


Fig. 9: This plot shows the effect of using shared parameters across the layers of the unfolded network for a 16×16 MIMO system for independent Rayleigh channels.

Fig. 10: This plot shows the effect of varying the number of layers in JED-U-ADMM in a 16×16 MIMO system for independent Rayleigh channels.

for 32×32 MIMO in Fig. 11 (b), we get an SNR improvement of 4 dB for a BER of 10^{-2} . Comparing in terms of BER

obtained at a given SNR, we see that for the 16×16 MIMO in Fig. 11 (a), JED-U-ADMM needs 10 layers to reach BER $\approx 10^{-3}$ at SNR = 16 dB, which is an order of improvement

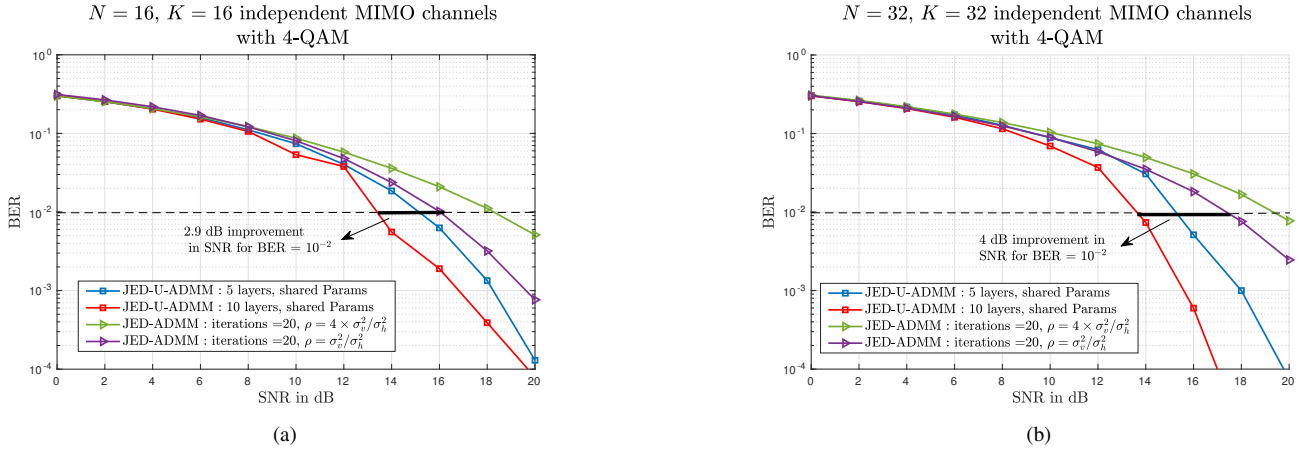


Fig. 11: This plot shows the effect of deep unfolding on the variation of BER vs SNR for (a) 16×16 and (b) 32×32 MIMO for independent Rayleigh channels.

over JED-ADMM that requires 20 iterations to give a BER $\approx 10^{-2}$ at the same SNR. We also note that for 16×16 MIMO in Fig. 11 (a), JED-U-ADMM with 5 layers has almost similar performance as JED-ADMM with 20 iterations and $\rho = \sigma_v^2 / \sigma_h^2$. On the other hand, Fig. 11 (b) shows that for 32×32 MIMO system, even 5 layers of JED-U-ADMM shows more than 2 dB SNR improvement for SNR > 14 dB. Thus, as we increase the system size, deep unfolding seems to perform much better than conventional iterative methods.

Experiment 7: Study the effect of varying the ratio N/K in an unfolded network in the presence of independent MIMO channels.

This experiment showcases the performance of JED-U-ADMM when we operate in the standard MIMO regime of $N > K$ and in the overloaded MIMO regime of $N < K$.

For $N > K$ (the standard MIMO regime), we had observed from Fig. 5 that JED-ADMM needs a large number of iterations of about 100 to outperform JED-AM. However, with deep unfolding, we can improve the performance, especially at high SNR values by about 1 dB, as compared to JED-ADMM, with even 10 layers as shown in Fig. 12 (a).

For the overloaded MIMO in Fig. 12 (b), we see that JED-U-ADMM needs only 10 layers to consistently yield a lower BER than JED-ADMM. At SNR = 20 dB, JED-U-ADMM with 10 layers gives a 2 dB improvement in SNR compared to 20 iterations of JED-ADMM. As an example, at SNR = 22 dB, we need 20 iterations of JED-ADMM yield a BER of 10^{-2} whereas even 10 layers of JED-U-ADMM gives us BER $< 10^{-3}$.

Experiment 8: Study the effect of correlation ρ_c at the receiver antennas for unfolded network with $N \geq K$. In this experiment, we demonstrate the performance of JED-ADMM and JED-U-ADMM, for the case of correlated channels. We consider the Kronecker correlation channel model [41] with the correlation coefficient ρ_c at the receiver.

We observe from Fig. 13 that as the correlation at the receiver antennas increases, both JED-ADMM and JED-U-

ADMM degrade in performance. For the case of 16×16 MIMO, we compare 5 layers of JED-U-ADMM with 20 iterations of JED-ADMM in 13 (a). We see that for $\rho_c = 0.1$, using unfolding results in slightly lesser BER of JED-U-ADMM than JED-ADMM, with the difference being more prominent at higher SNR > 16 dB. However, for $\rho_c = 0.5$ and 0.9 , the BER curves of JED-U-ADMM and JED-ADMM are almost the same.

In Fig. 13 (b), we present the BER curves for 32×32 with 10 layers of JED-U-ADMM and 20 iterations of JED-ADMM. For $\rho_c = 0.1$ and 0.5 , we see that unfolding improves the BER performance throughout the range of SNR values presented, whereas for $\rho_c = 0.9$, the improvement is visible only for SNR > 10 dB.

Experiment 9: Study the effect of unfolding for a fixed $K = 16$ and varying N in the presence of independent MIMO channels.

We study the performance of the proposed algorithms by fixing the number of UEs $K = 16$ and vary the number of BS antennas $N = 8, 16, 32, 48, 64$.

As N increases, the system transitions from an overloaded scenario to the standard MIMO yielding a lower BER. As N is increased from 16 to 32, the BER falls drastically from $\approx 10^{-2}$ to $\approx 10^{-5}$ at SNR = 14 dB. Upon further increasing N to 48 and 64, we note that the margin of improvement in performance gradually reduces.

We now present a summary of the observations in the next section.

VII. DISCUSSION AND CONCLUSION

In this paper, we propose two algorithms for Joint Channel Estimation and Symbol Detection, JED-ADMM and its unfolded version, JED-U-ADMM. The ADMM based algorithms for symbol detection exploit the non-smooth constraint arising from the QAM structure of the data symbols which significantly improve the BER performance compared to the

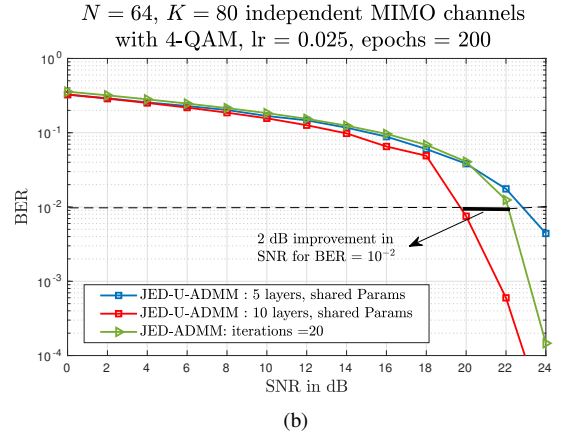
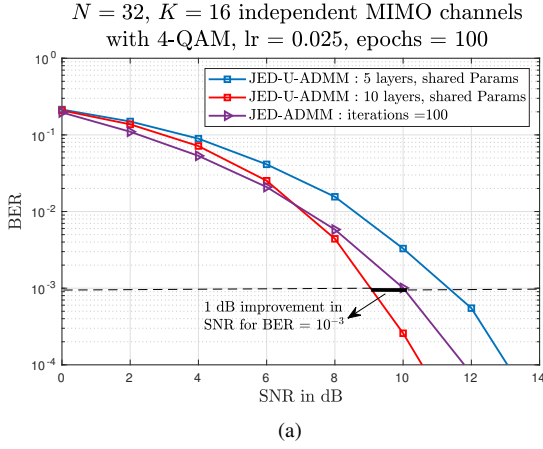


Fig. 12: This plot shows the variation of BER vs SNR for (a) $N > K : 32 \times 16$ MIMO and (b) $N < K : 64 \times 80$ for independent Rayleigh channels.

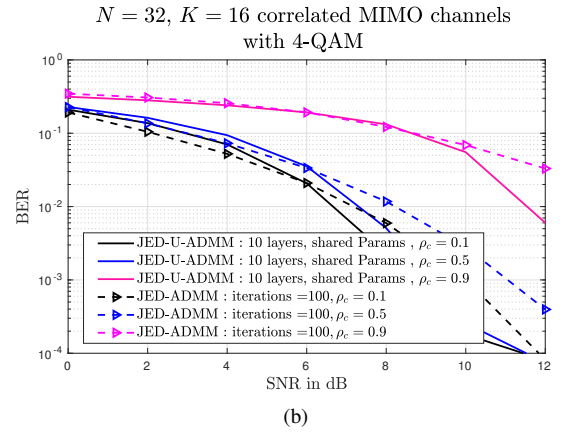
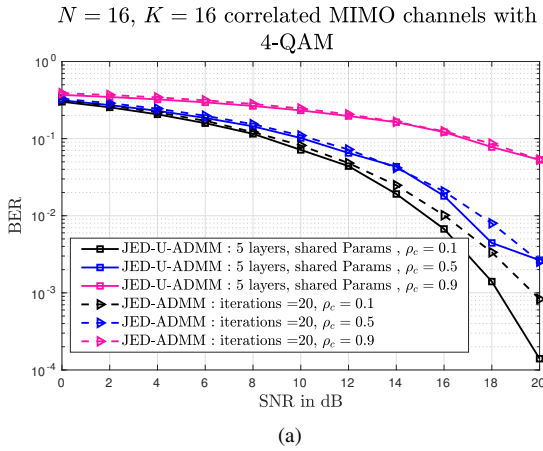


Fig. 13: This plot shows the variation of BER vs SNR for (a) 16×16 and (b) 32×16 MIMO where the channels are correlated at the Rx with ρ_c (22) for correlated channels [41].

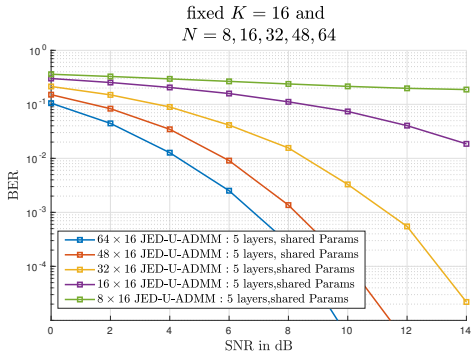


Fig. 14: This plot shows the variation of BER vs SNR for $K = 16, N = 8, 16, 32, 48, 64$ MIMO for independent Rayleigh channels.

state-of-the-art JED-AM. We provide a summary our findings, as per the experiments conducted.

Considering the fully loaded MIMO $N = K$, our proposed algorithm JED-ADMM, in Algorithm 2, results in an SNR improvement of about 3 dB for $\text{BER} = 10^{-2}$ for $\rho = \frac{\sigma_v^2}{\sigma_h^2}$ chosen,

as shown in Fig. 4. The unfolded algorithm JED-U-ADMM, in Algorithm 3, further provides 3-4 dB SNR improvement over JED-ADMM as shown in Fig. 11 (a), thereby demonstrating the power of model-based neural network architectures. For the standard MIMO regime $N > K$, JED-U-ADMM needs only 10 iterations to outperform 100 iterations of JED-ADMM, by giving an SNR improvement of 1 dB whereas JED-ADMM requires (~ 100) iterations to yield an an SNR improvement of 0.5 dB over JED-AM, as depicted in Fig. 5. In the overloaded scenario $N < K$, we note from Fig. 6 that JED-ADMM continues to exhibit waterfall decrease in BER whereas JED-AM saturates around $\text{BER} = 2 \times 10^{-2}$. Fig. 12 (b) depicts an additional SNR improvement of 2 dB by JED-U-ADMM. Furthermore, under correlated channel model in Fig. 8, JED-ADMM markedly lowers the BER, especially for lower values of ρ_c . The unfolded network JED-U-ADMM further leads to slight improvement in BER performance over JED-ADMM in Fig. 13.

Hence, we conclude that both of our proposed algorithms JED-ADMM and JED-U-ADMM enhance the BER perfor-

mance in MIMO communication systems over the existing JED technique in [18]. The deep unfolded network JED-U-ADMM provides us with an additional SNR gain over the iterative JED-ADMM in much fewer iterations ≤ 10 , thus reducing the computational complexity. The unfolded network contains few trainable parameters and has simple update equations. In our future work, we plan to extend the proposed scheme to higher orders of modulation.

REFERENCES

- [1] E. Björnson, E. G. Larsson, and T. L. Marzetta, "Massive MIMO: ten myths and one critical question," *IEEE Communications Magazine*, vol. 54, no. 2, pp. 114–123, 2016.
- [2] Abhishek, A. K. Sah, and A. K. Chaturvedi, "Improved sparsity behaviour and error localization in detectors for large MIMO systems," in *IEEE Globecom Workshops (GC Wkshps)*, 2016, pp. 1–6.
- [3] E. C. Marques, N. Maciel, L. Naviner, H. Cai, and J. Yang, "A review of sparse recovery algorithms," *IEEE Access*, vol. 7, pp. 1300–1322, 2018.
- [4] R. Ran, J. Wang, S. K. Oh, and S. N. Hong, "Sparse-aware minimum mean square error detector for MIMO systems," *IEEE Communications Letters*, vol. 21, no. 10, pp. 2214–2217, 2017.
- [5] R. Hayakawa and K. Hayashi, "Convex optimization-based signal detection for massive overloaded MIMO systems," *IEEE Transactions on Wireless Communications*, vol. 16, no. 11, pp. 7080–7091, 2017.
- [6] S. Takabe, M. Imanishi, T. Wadayama, and K. Hayashi, "Deep learning-aided projected gradient detector for massive overloaded mimo channels," in *IEEE International Conference on Communications (ICC)*, 2019, pp. 1–6.
- [7] N. T. Nguyen, K. Lee, and H. Dai, "Application of deep learning to sphere decoding for large MIMO systems," *IEEE Transactions on Wireless Communications*, vol. 20, no. 10, pp. 6787–6803, 2021.
- [8] M. A. Albreem, A. H. Alhabbash, S. Shahabuddin, and M. Juntti, "Deep learning for massive MIMO uplink detectors," *IEEE Communications Surveys & Tutorials*, vol. 24, no. 1, pp. 741–766, 2021.
- [9] C. Jeon, R. Ghods, A. Maleki, and C. Studer, "Optimality of large MIMO detection via approximate message passing," in *2015 IEEE International Symposium on Information Theory (ISIT)*. IEEE, 2015, pp. 1227–1231.
- [10] Z.-Q. Luo, W.-K. Ma, A. M.-C. So, Y. Ye, and S. Zhang, "Semidefinite relaxation of quadratic optimization problems," *IEEE Signal Processing Magazine*, vol. 27, no. 3, pp. 20–34, 2010.
- [11] A. Balatsoukas-Stimming and C. Studer, "Deep unfolding for communications systems: A survey and some new directions," in *IEEE International Workshop on Signal Processing Systems (SiPS)*. IEEE, 2019, pp. 266–271.
- [12] N. Samuel, T. Diskin, and A. Wiesel, "Deep MIMO detection," in *IEEE 18th International Workshop on Signal Processing Advances in Wireless Communications (SPAWC)*. IEEE, 2017, pp. 1–5.
- [13] H. He, C.-K. Wen, S. Jin, and G. Y. Li, "Model-driven deep learning for MIMO detection," *IEEE Transactions on Signal Processing*, vol. 68, pp. 1702–1715, 2020.
- [14] K. Ghavami and M. Naraghi-Pour, "Blind channel estimation and symbol detection for multi-cell massive MIMO systems by expectation propagation," *IEEE Transactions on Wireless Communications*, vol. 17, no. 2, pp. 943–954, 2018.
- [15] J. Zhang, X. Yuan, and Y.-J. A. Zhang, "Blind signal detection in massive MIMO: Exploiting the channel sparsity," *IEEE Transactions on Communications*, vol. 66, no. 2, pp. 700–712, 2018.
- [16] X. Kuai, X. Yuan, W. Yan, H. Liu, and Y. J. Zhang, "Double-sparsity learning-based channel-and-signal estimation in massive MIMO with generalized spatial modulation," *IEEE Transactions on Communications*, vol. 68, no. 5, pp. 2863–2877, 2020.
- [17] W. Yan and X. Yuan, "Semi-blind channel-and-signal estimation for uplink massive MIMO with channel sparsity," *IEEE Access*, vol. 7, pp. 95 008–95 020, 2019.
- [18] B. B. Yilmaz and A. T. Erdogan, "Channel estimation for massive MIMO: A semiblind algorithm exploiting qam structure," in *2019 53rd Asilomar Conference on Signals, Systems, and Computers*, 2019, pp. 2077–2081.
- [19] K. Gregor and Y. LeCun, "Learning fast approximations of sparse coding," in *Proceedings of the 27th International Conference on International Conference on Machine Learning*, 2010, p. 399–406.
- [20] Y. Li, M. Tofighi, J. Geng, V. Monga, and Y. C. Eldar, "Efficient and interpretable deep blind image deblurring via algorithm unrolling," *IEEE Transactions on Computational Imaging*, vol. 6, pp. 666–681, 2020.
- [21] Y. Yang, J. Sun, H. Li, and Z. Xu, "ADMM-CSNet: A deep learning approach for image compressive sensing," *IEEE Transactions on Pattern Analysis and Machine Intelligence*, vol. 42, no. 3, pp. 521–538, 2020.
- [22] K. Zhang, L. Van Gool, and R. Timofte, "Deep unfolding network for image super-resolution," in *IEEE/CVF Conference on Computer Vision and Pattern Recognition (CVPR)*. IEEE, 2020, pp. 3214–3223.
- [23] V. Monga, Y. Li, and Y. C. Eldar, "Algorithm unrolling: Interpretable, efficient deep learning for signal and image processing," *IEEE Signal Processing Magazine*, vol. 38, no. 2, pp. 18–44, 2021.
- [24] H. Song, X. You, C. Zhang, and C. Studer, "Soft-output joint channel estimation and data detection using deep unfolding," in *2021 IEEE Information Theory Workshop (ITW)*, 2021, pp. 1–5.
- [25] M. Khani, M. Alizadeh, J. Hoydis, and P. Fleming, "Adaptive neural signal detection for massive MIMO," *IEEE Transactions on Wireless Communications*, vol. 19, no. 8, pp. 5635–5648, 2020.
- [26] H. He, C.-K. Wen, S. Jin, and G. Y. Li, "A model-driven deep learning network for MIMO detection," in *IEEE Global Conference on Signal and Information Processing (GlobalSIP)*. IEEE, 2018, pp. 584–588.
- [27] S. Khobahi, N. Shlezinger, M. Soltanalian, and Y. C. Eldar, "Lord-net: Unfolded deep detection network with low-resolution receivers," *IEEE Transactions on Signal Processing*, vol. 69, pp. 5651–5664, 2021.
- [28] G. Marti and C. Studer, "Mitigating smart jammers in MU-MIMO via joint channel estimation and data detection," in *ICC 2022 - IEEE International Conference on Communications*, 2022, pp. 1336–1342.
- [29] H. Song, T. Goldstein, X. You, C. Zhang, O. Tirkkonen, and C. Studer, "Joint channel estimation and data detection in cell-free massive MU-MIMO systems," *IEEE Transactions on Wireless Communications*, vol. 21, no. 6, pp. 4068–4084, 2022.
- [30] K. Kang, Q. Hu, Y. Cai, G. Yu, J. Hoydis, and Y. C. Eldar, "Mixed-timescale deep-unfolding for joint channel estimation and hybrid beamforming," *IEEE Journal on Selected Areas in Communications*, vol. 40, no. 9, pp. 2510–2528, 2022.
- [31] L. Xu, F. Gao, T. Zhou, S. Ma, and W. Zhang, "Joint channel estimation and mixed-ADCs allocation for massive MIMO via deep learning," *IEEE Transactions on Wireless Communications*, vol. 22, no. 2, pp. 1029–1043, 2023.
- [32] M.-W. Un, M. Shao, W.-K. Ma, and P. Ching, "Deep MIMO detection using ADMM unfolding," in *2019 IEEE Data Science Workshop (DSW)*. IEEE, 2019, pp. 333–337.
- [33] P. Sabeti, A. Farhang, I. Macaluso, N. Marchetti, and L. Doyle, "Blind channel estimation for massive MIMO: A deep learning assisted approach," in *IEEE International Conference on Communications (ICC)*, 2020, pp. 1–6.
- [34] Y. Zhang, J. Sun, J. Xue, G. Y. Li, and Z. Xu, "Deep expectation-maximization for joint mimo channel estimation and signal detection," *IEEE Transactions on Signal Processing*, vol. 70, pp. 4483–4497, 2022.
- [35] S. Boyd, N. Parikh, and E. Chu, *Distributed optimization and statistical learning via the alternating direction method of multipliers*. Now Publishers Inc, 2011.
- [36] S. Shahabuddin, I. Hautala, M. Juntti, and C. Studer, "Admm-based infinity-norm detection for massive mimo: Algorithm and vlsi architecture," *IEEE Transactions on Very Large Scale Integration (VLSI) Systems*, vol. 29, no. 4, pp. 747–759, 2021.
- [37] Y. Li, M. Tofighi, V. Monga, and Y. C. Eldar, "An algorithm unrolling approach to deep image deblurring," in *IEEE International Conference on Acoustics, Speech and Signal Processing (ICASSP)*. IEEE, 2019, pp. 7675–7679.
- [38] S. Bhattacharya, K. V. S. Hari, and Y. C. Eldar, "Joint channel estimation and symbol detection in overloaded MIMO using ADMM," in *2023 IEEE Statistical Signal Processing Workshop (SSP)*, accepted for publication.
- [39] A. Paszke, S. Gross, F. Massa, A. Lerer, J. Bradbury, G. Chanan, T. Killeen, Z. Lin, N. Gimelshein, L. Antiga et al., "Pytorch: An imperative style, high-performance deep learning library," *Advances in neural information processing systems*, vol. 32, 2019.
- [40] D. P. Kingma and J. Ba, "Adam: A method for stochastic optimization," *arXiv preprint arXiv:1412.6980*, 2014.
- [41] C. Oestges, "Validity of the kronecker model for MIMO correlated channels," in *IEEE 63rd Vehicular Technology Conference*, vol. 6. IEEE, 2006, pp. 2818–2822.